Satellite Observations of Earth's Energy Budget and Climate: Past, Present and Future

Norman G. Loeb, T. Thorsen, H. Wang, W. Su, and S. Kato
NASA Langley Research Center, Hampton, VA

15th Conference on Atmospheric Radiation, July 9, 2018, Vancouver, BC

Outline

1) A brief history of Earth Radiation Budget Observation & Future Prospects

2) ERB Science Focus Areas: Selected Highlights

3) Recent Changes in TOA ERB

Pre-Satellite Years: First Earth Radiation Budget Diagram (1908)

SW

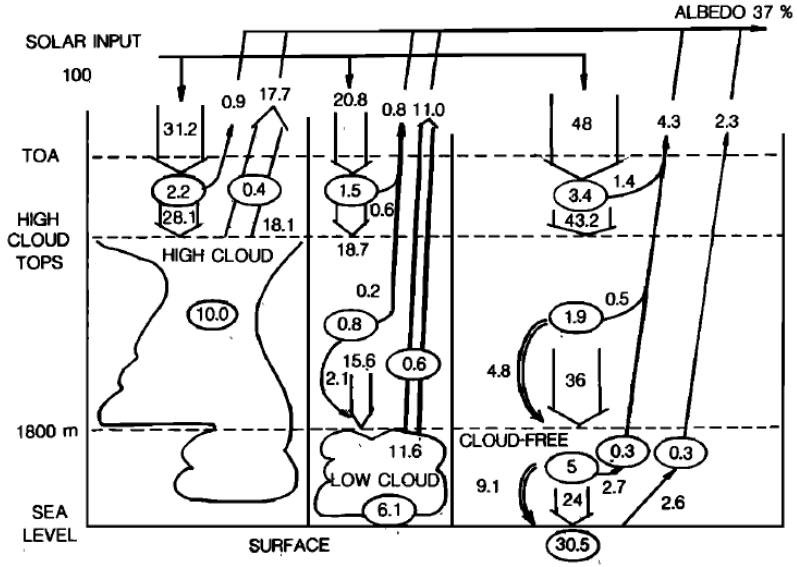

Fig. 1*a*. Shortwave components of the earth radiation budget, following *Abbot and Fowle* [1908*a*, *b*]. All figures are in percent of the global annual mean incident solar flux $S/4$. Circled figures correspond to absorption and have been made consistent with the transmission and reflection given for the different atmospheric layers. The result is that the total absorption below 1800 m is 42.2% and not 44.9% as given by Abbot and Fowle.

LW

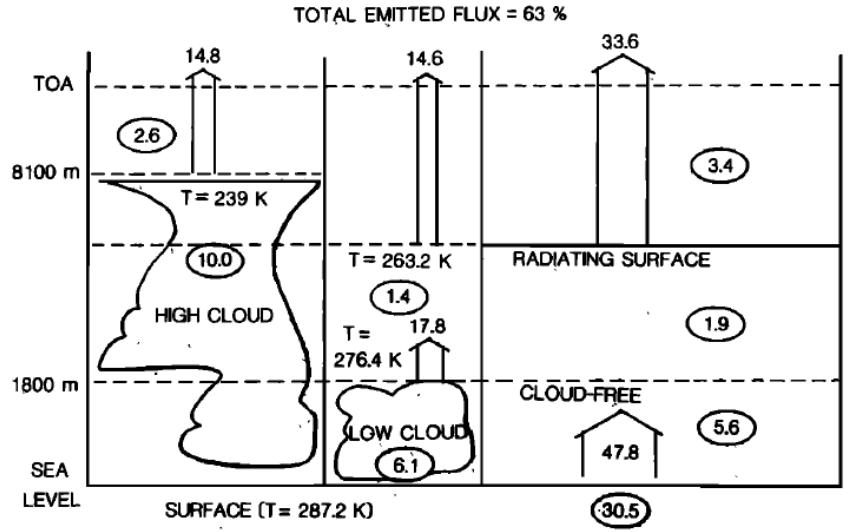

Fig. 1*b*. Interpretation of the upward long-wave components of the earth radiation budget, following *Abbot and Fowle* [1908*a*, *b*], consistent with $S = 1457.4$ W m^{-2}, $\sigma = 0.37$, and a Stefan-Boltzmann constant of $\sigma = 5.36 \times 10^{-8}$ W m^{-2} K^{-4}.

$S_o = 1457.4$ Wm^{-2}

$\alpha = 0.37$

OLR = 230 Wm^{-2}

Early Satellite Years

- October 1957: Soviet Union launched the world's first artificial satellite: Sputnik 1.
- NASA Explorer 6 launches on February 17, 1959.
- NASA Explorer 7 satellite was launched in 1959 with a set of detectors for measuring radiation from Earth.
- This experiment by Vern Suomi was the first instrument to study weather and climate from space.

Front Page of NY Times, Feb 18, 1959

ork Times.

LATE CITY EDITION
U. S. Weather Bureau Report (Page 46): Forecasts: Cloudy, some rain today. Fair and cold tomorrow. Temp. range: 41—37. Yesterday: 48.4 - 33.6.

FEBRUARY 18, 1959. 10 cents beyond 50-mile zone from New York City except on Long Island. Higher in air delivery cities. FIVE CENTS

Rocket Launches a Weather-Observation Satellite

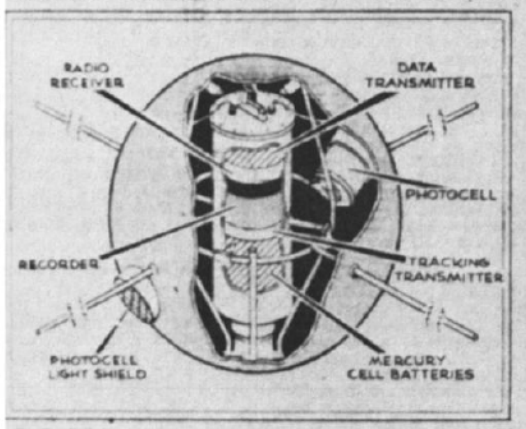

The New York Times Feb. 18, 1959
Drawing shows some of the instruments enclosed in the 20-inch satellite. They are designed to provide first pictures taken from space of the earth's cloud cover.

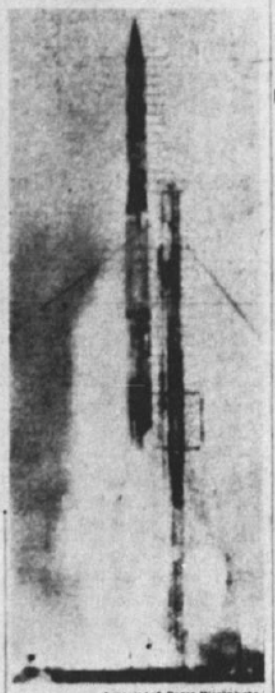

Associated Press Wirephoto
Vanguard rocket rises from its pad at Cape Canaveral.

VANGUARD FIRES SATELLITE IN ORBIT TO SCAN WEATHER

Vehicle Tops Expectation in Placing First Meteorology Observatory in Space

EISENHOWER HAILS FEAT

Sphere Functions Well on First Trip Around Earth on Cloud-Cover Study

By JOHN W. FINNEY
Special to The New York Times.

WASHINGTON, Feb. 17—The United States launched into orbit today a scientific satellite that will serve as man's first weather observation station in space.

The 20-inch, 21½-pound spherical satellite was launched from Cape Canaveral, Fla., by the Navy's Project Vanguard, which had put only one satellite into orbit in several attempts.

Fig. 1. The front page of the *New York Times* announced the launch of Explorer 6 satellite on February 17, 1959.

Early Satellite Years

Explorer 7 Satellite With Hemispherical Radiometers

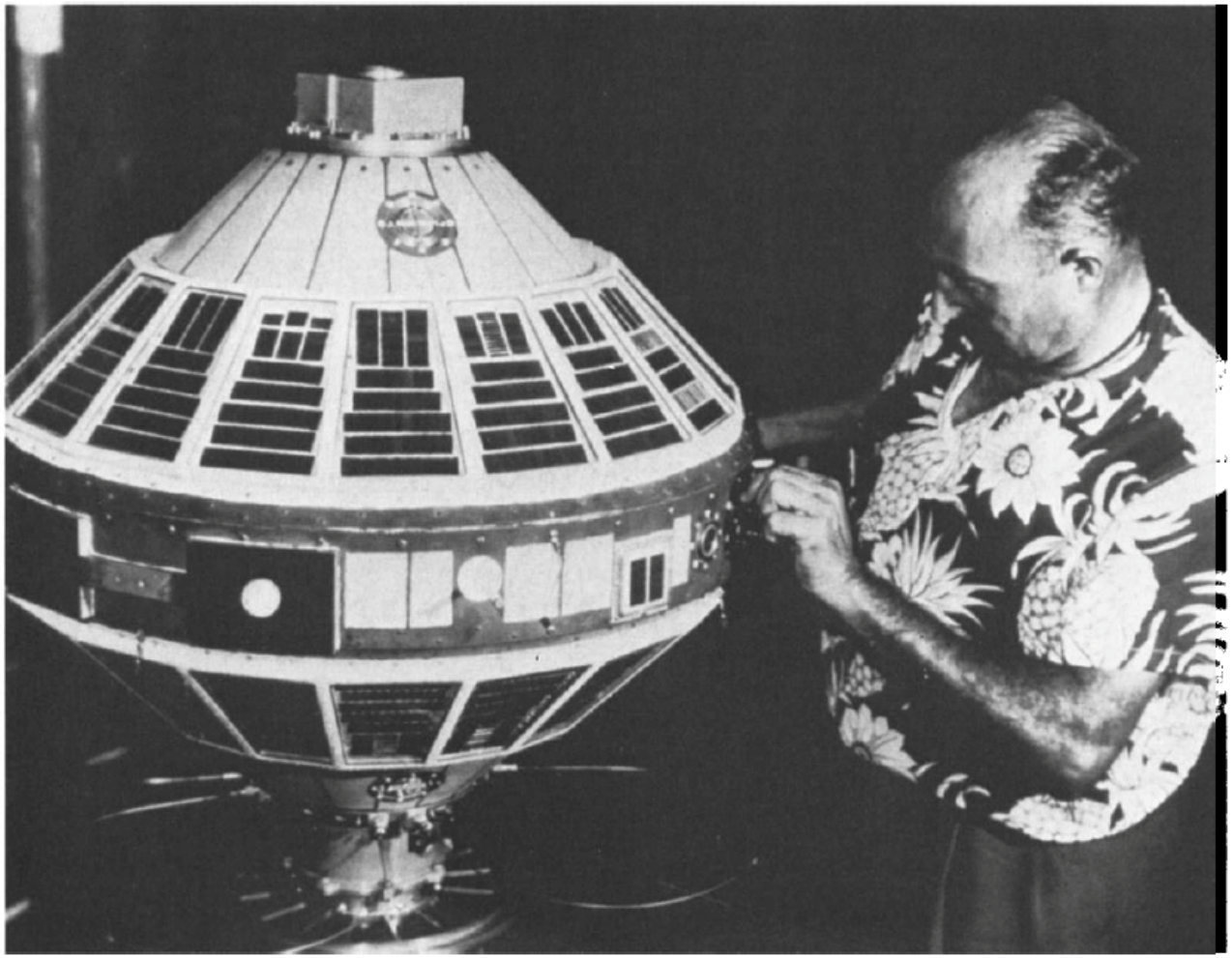

Fig. 3. Explorer 7 satellite with hemispherical radiometers at its equator to monitor the ERB [*Suomi*, 1957].

ERB Science Addressed by ERB Observations

- **ERB observations provide critical data for:**

1) Quantifying how the heat uptake of the planet changes on timescales ranging from monthly to decadal.

2) Constraining climate model projections of future warming by narrowing uncertainty in cloud feedback.

3) Quantifying Aerosol Radiative Forcing.

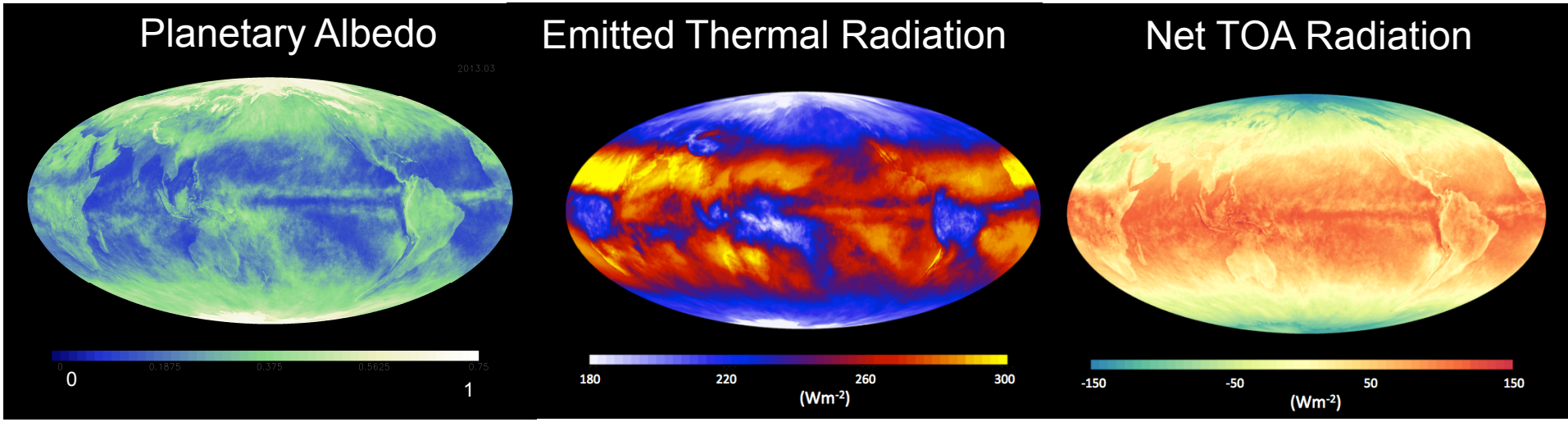

CERES Data Fusion

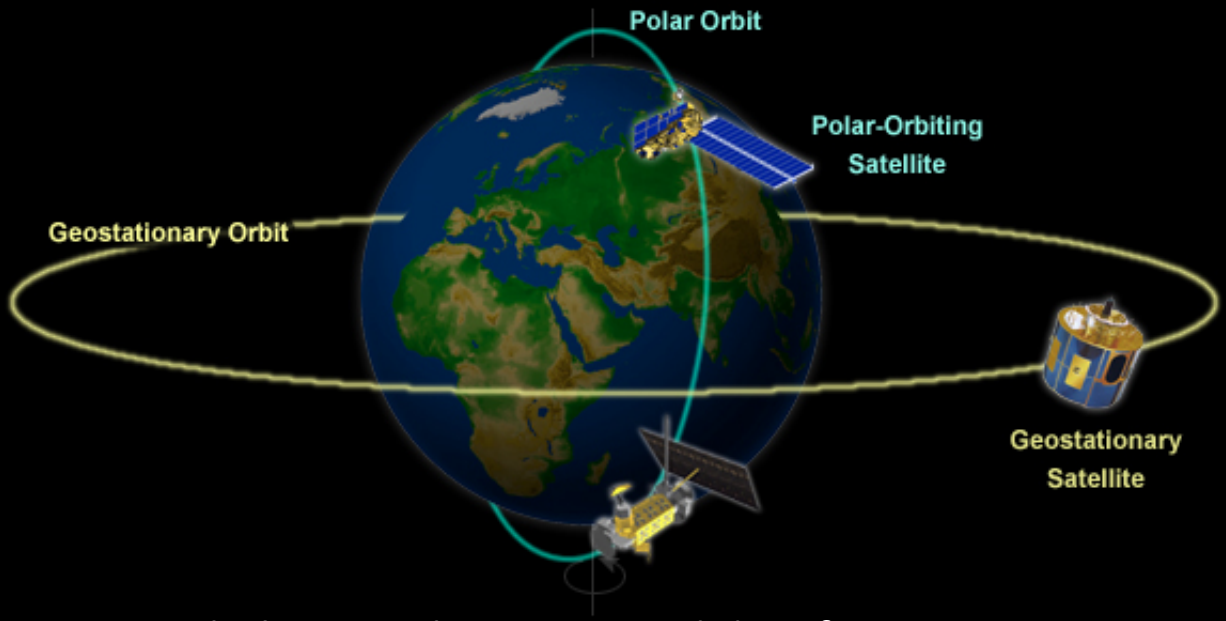

- During the CERES period, the team has processed data from:
  - 7 CERES instruments
  - 1 VIRS imager (TRMM)
  - 2 MODIS imagers (Terra, Aqua)
  - 2 VIIRS imagers (S-NPP, NOAA-20)
  - 18 geostationary imagers
  - Solar irradiance measurements
  - Meteorological, ozone and aerosol assimilation data
  - Snow/ice maps

➢ **All are integrated to obtain climate accuracy in radiative fluxes from the top to the bottom of the atmosphere.**

Earth's Energy Budget (1σ Range)

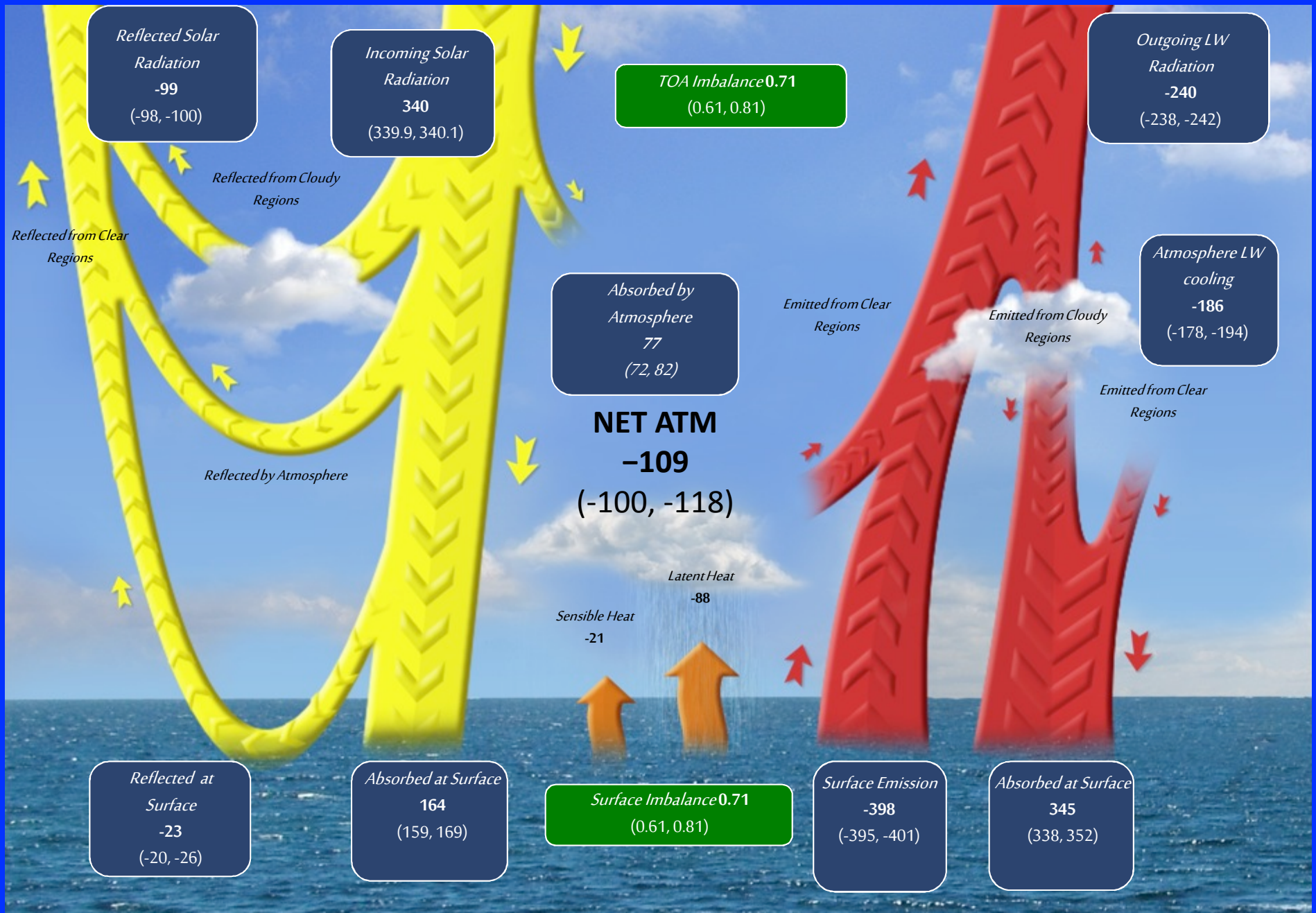

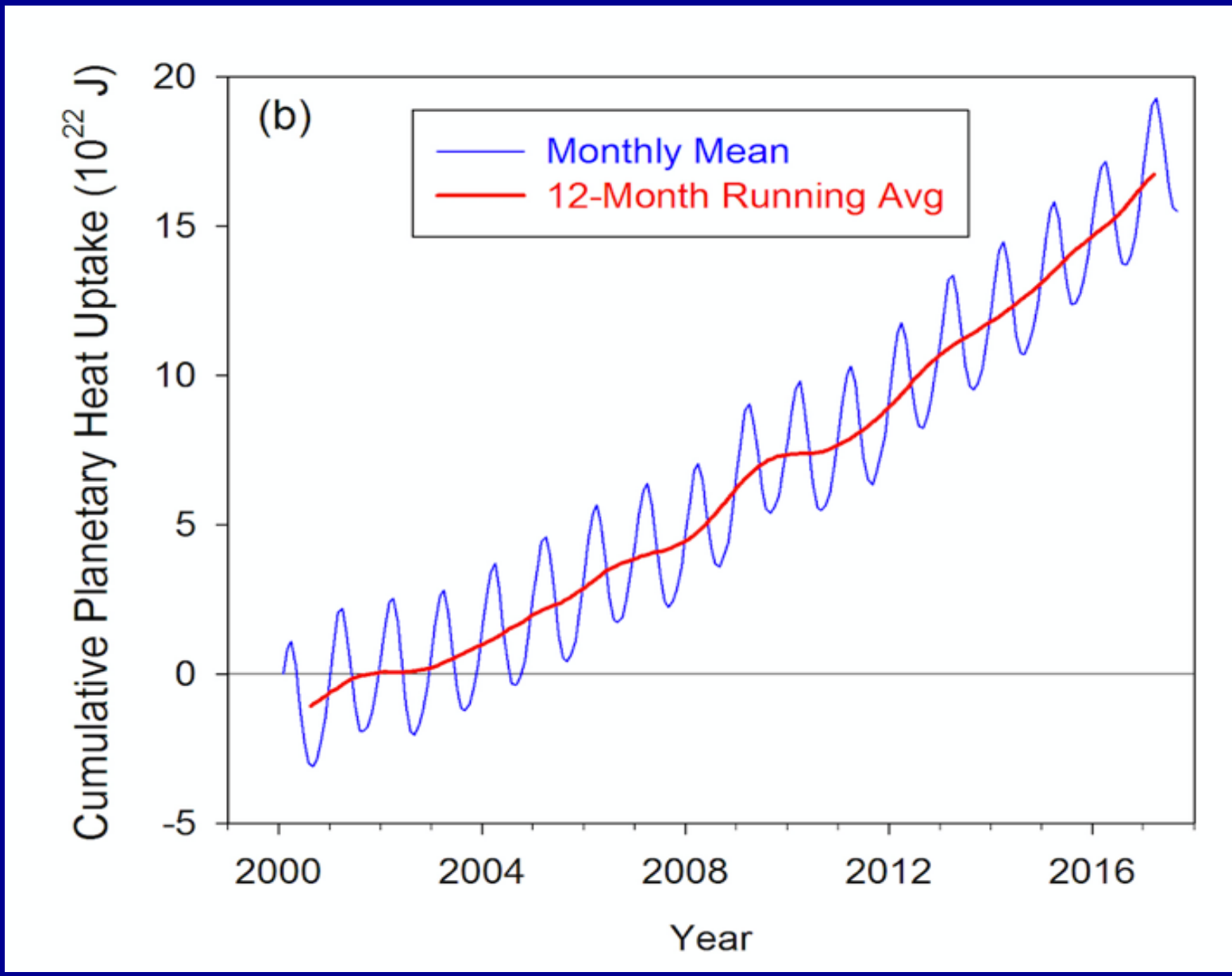
(b)
Monthly Mean
12-Month Running Avg
Cumulative Planetary Heat Uptake (10^{22} J)
20
15
10
5
0
-5
2000
2004
2008
2012
2016
Year

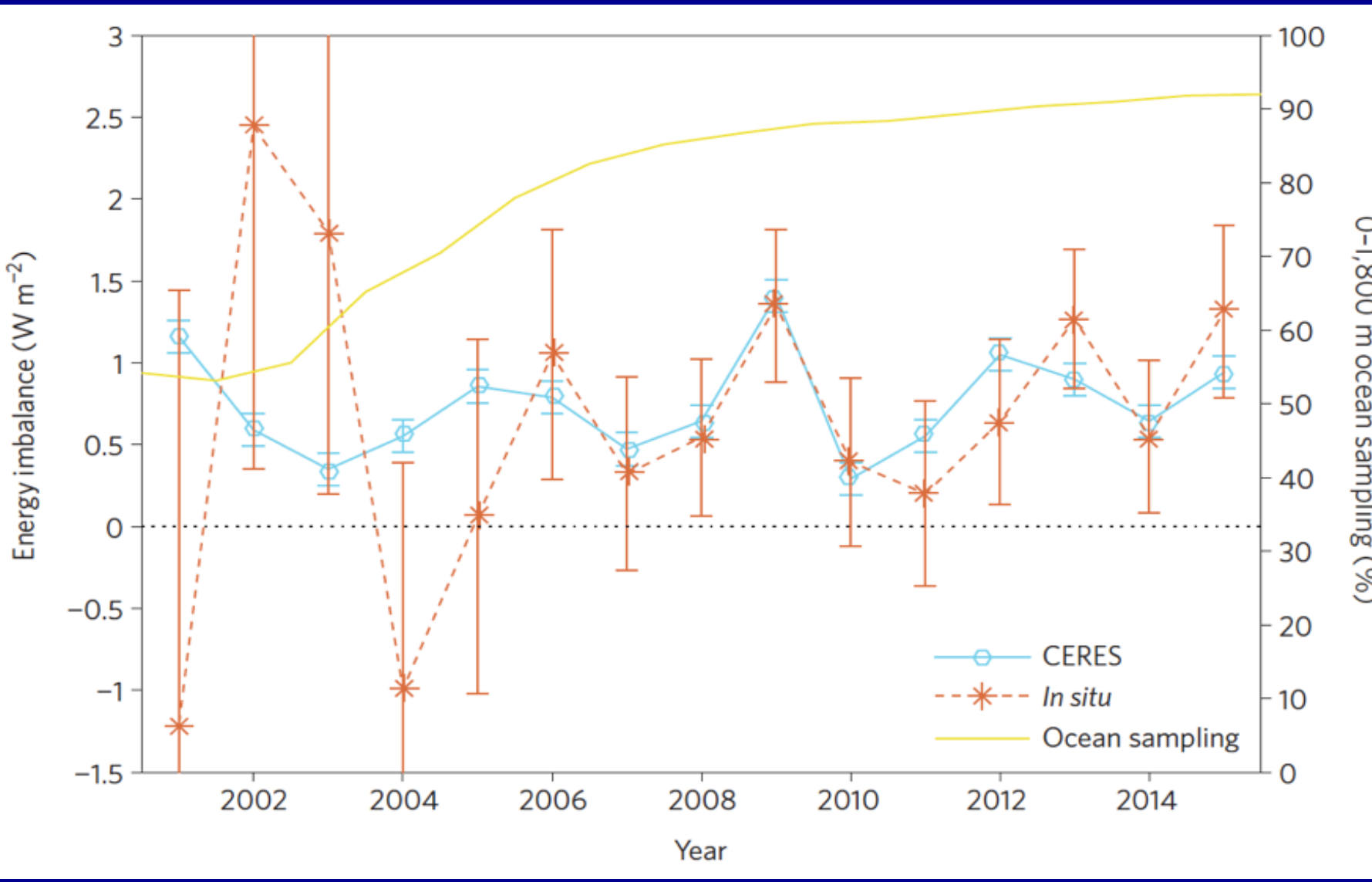
Energy imbalance (W m^{-2})
3
2.5
2
1.5
1
0.5
0
−0.5
−1
−1.5
2002
2004
2006
2008
2010
2012
2014
Year
100
90
80
70
60
50
40
30
20
10
0
0–1,800 m ocean sampling (%)
CERES
In situ
Ocean sampling

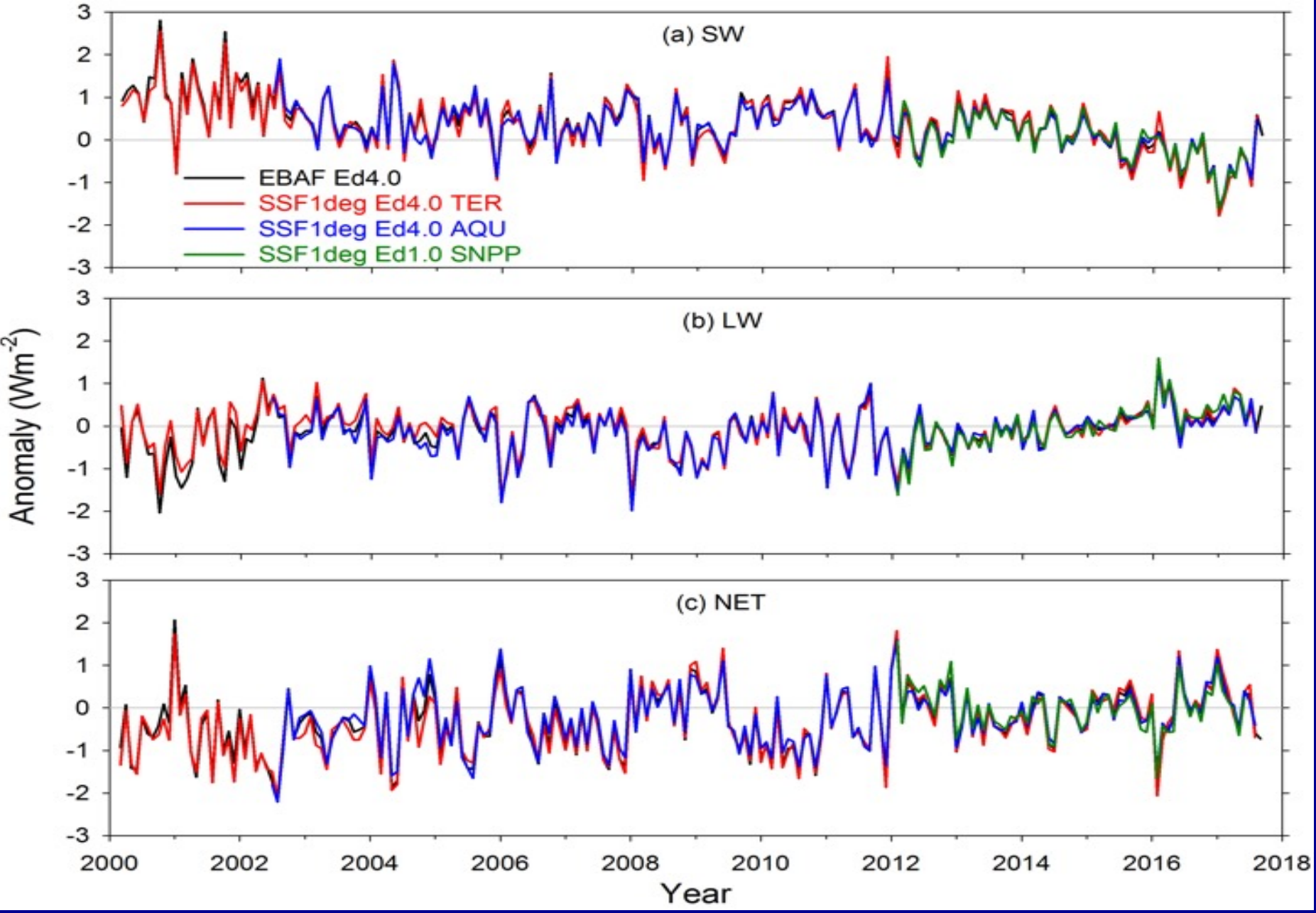
(a) SW
(b) LW
(c) NET
EBAF Ed4.0
SSF1deg Ed4.0 TER
SSF1deg Ed4.0 AQU
SSF1deg Ed1.0 SNPP
Anomaly (Wm-2)
Year
3
2
1
0
-1
-2
-3
2000
2002
2004
2006
2008
2010
2012
2014
2016
2018

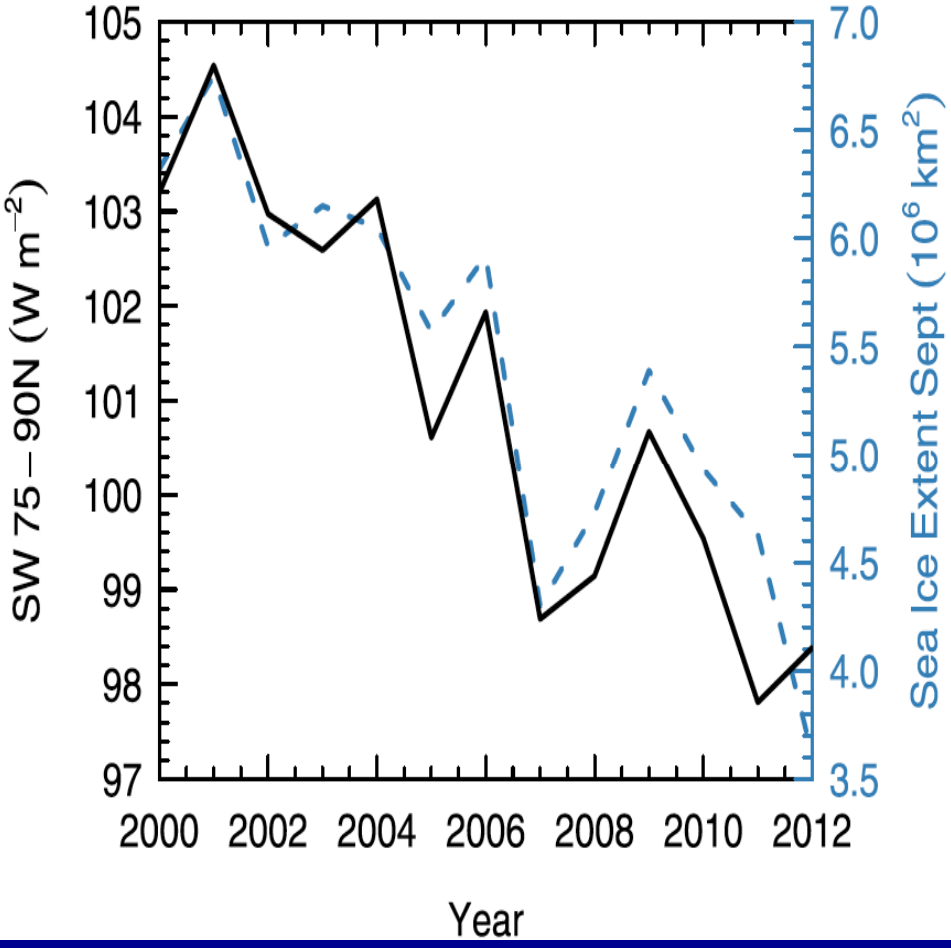
105
104
103
102
101
100
99
98
97
SW 75 – 90N (W m^{-2})
7.0
6.5
6.0
5.5
5.0
4.5
4.0
3.5
Sea Ice Extent Sept (10^6 km^2)
2000
2002
2004
2006
2008
2010
2012
Year

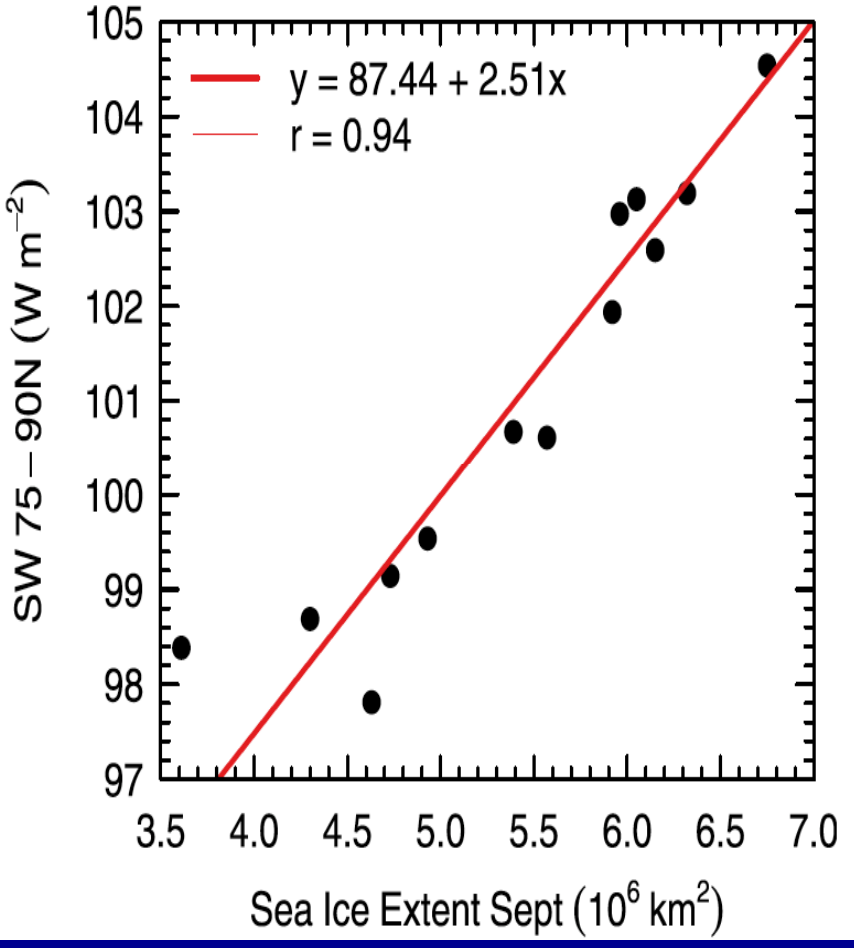
y = 87.44 + 2.51x
r = 0.94
105
104
103
102
101
100
99
98
97
SW 75 – 90N (W m^{-2})
3.5
4.0
4.5
5.0
5.5
6.0
6.5
7.0
Sea Ice Extent Sept (10^6 km^2)

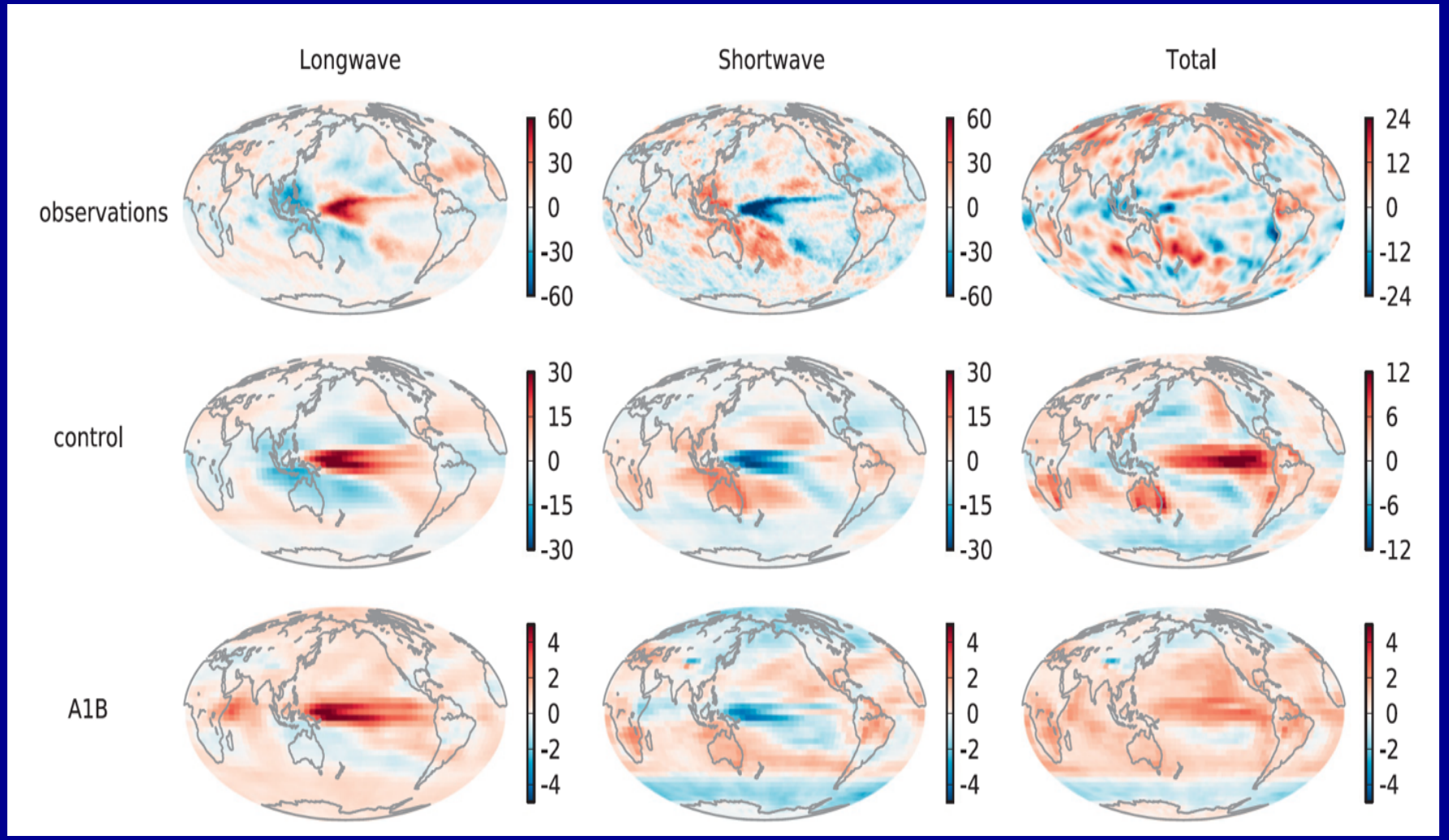
Longwave
Shortwave
Total
observations
control
A1B
60
30
0
-30
-60
24
12
-12
-24
15
-15
6
-6
4
2
-2
-4

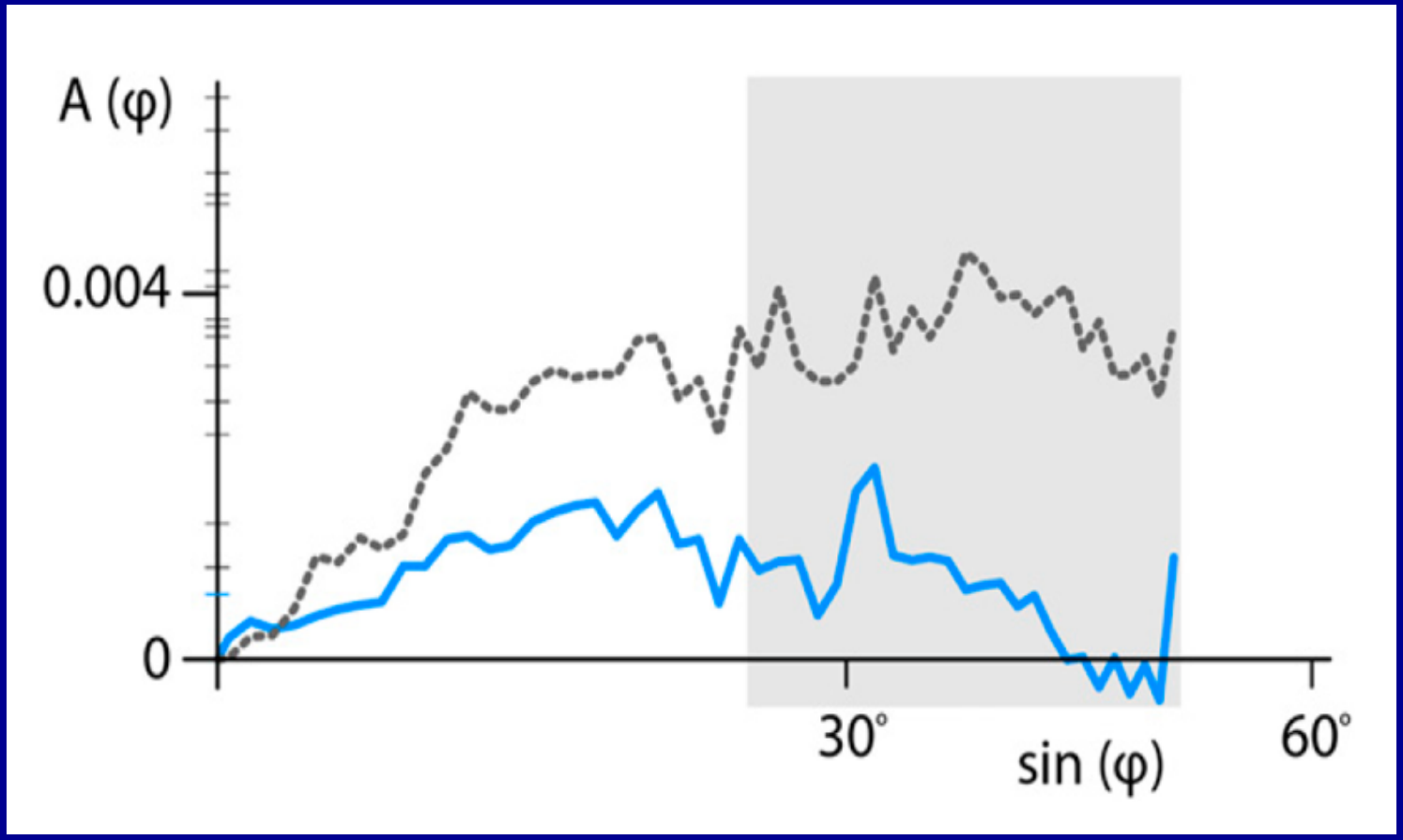
A (φ)
0.004
0
30°
sin (φ)
60°

Changes in Earth's Radiation Budget, Clouds & Aerosols,

Global and Annual Multi-Model Mean TOA Radiation for CMIP5 RCP Scenarios

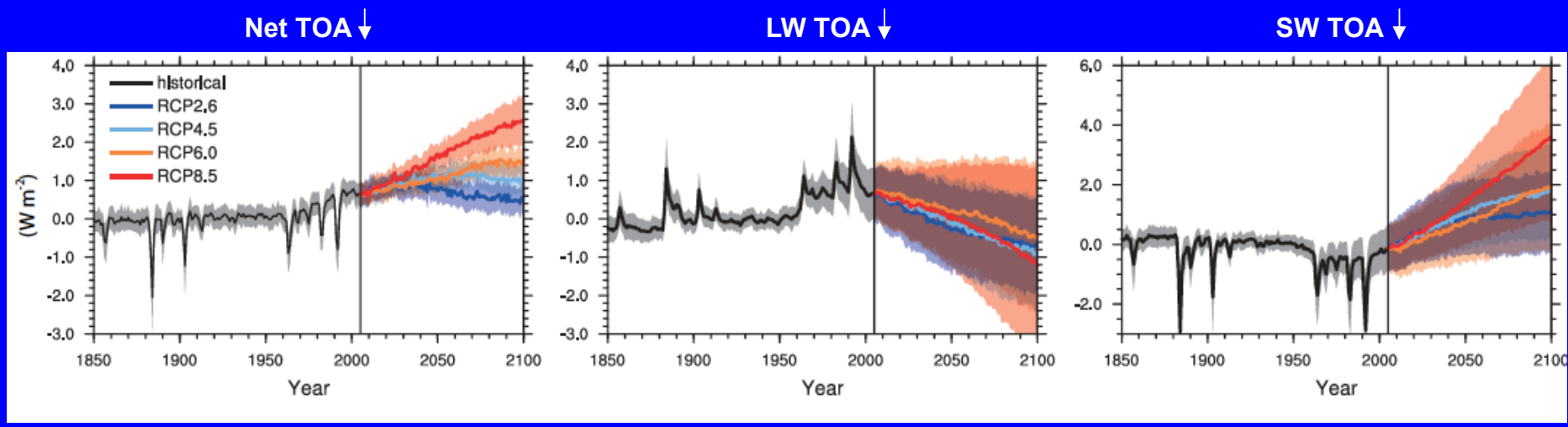

- TOA net radiative flux can either increase or decrease with surface temperature, depending upon the RCP scenario.
- For RCP8.5, the large increase in TOA absorbed SW radiation is due to cloud changes and changes in the cryosphere.

(AR5, 2013)

Decadal Variations in Net TOA Radiation, SST Trend and Ocean Heating Rate From Coupled Climate Model Simulations

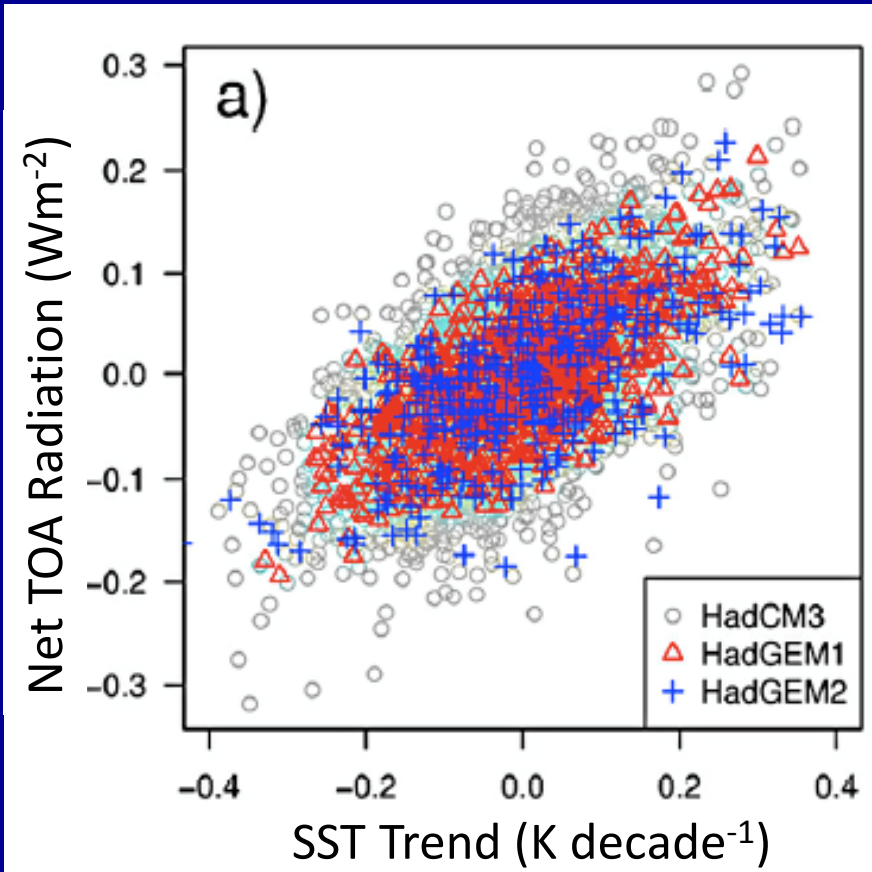

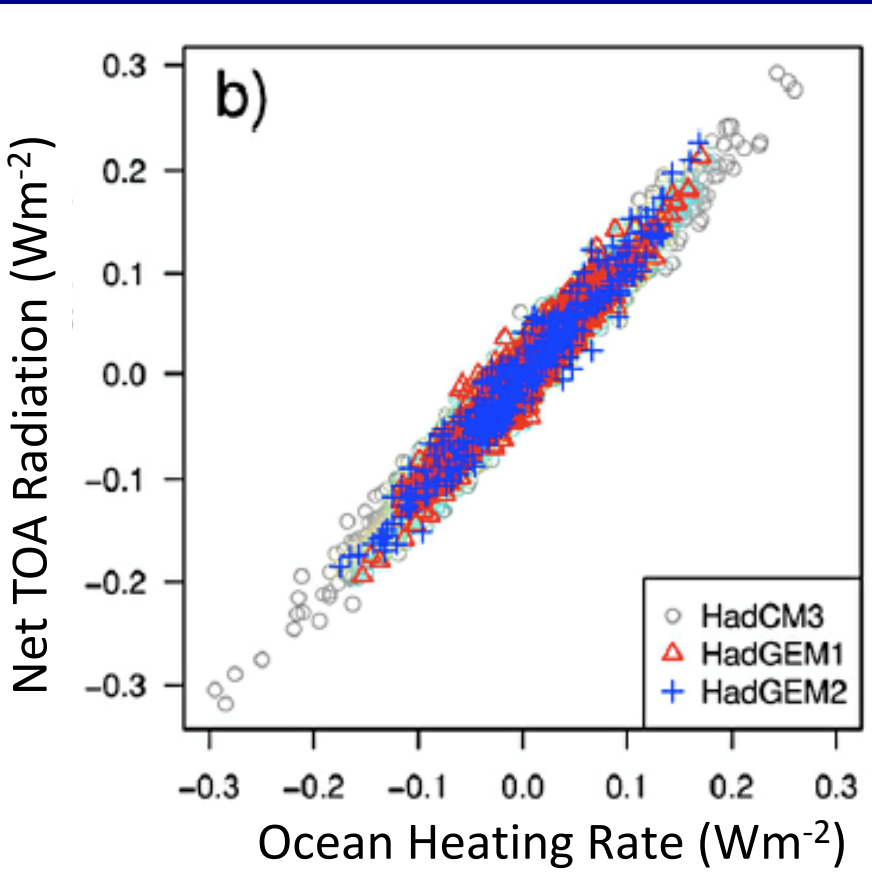

- Control run data from multi-century Met Office Hadley Centre climate model runs
- Approximately 30% of decades show a trend in net TOA radiation and SST that are of opposite sign.
- Ocean re-distribution of heat is the primary reason for the larger scatter seen between SST and total energy.

Palmer et al., GRL 2011

Earth's Heat Budget

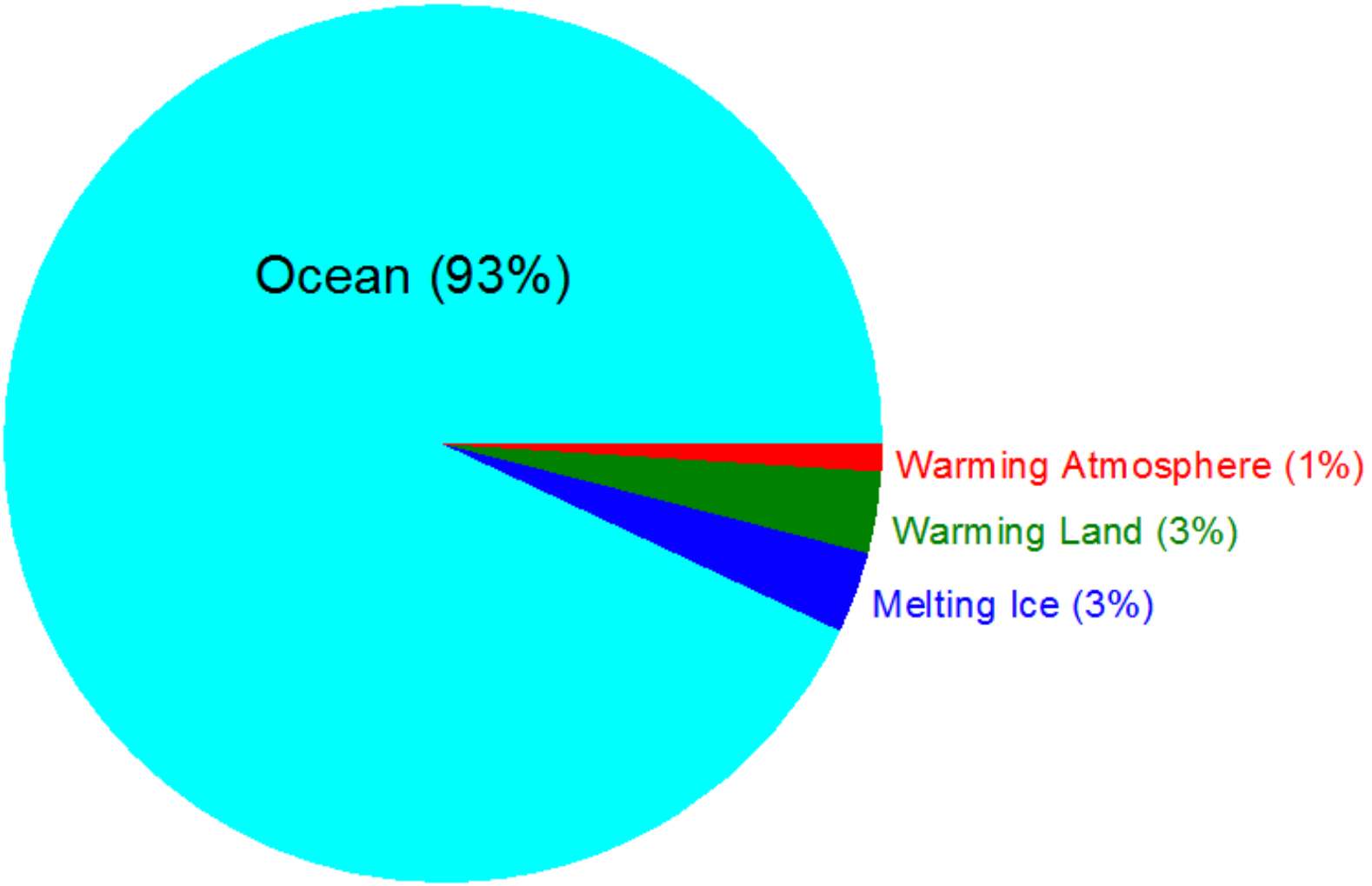

- Only 1% of the energy is used to change global mean surface temperature.
- Most of the excess heat in the climate system ends being stored in the ocean.

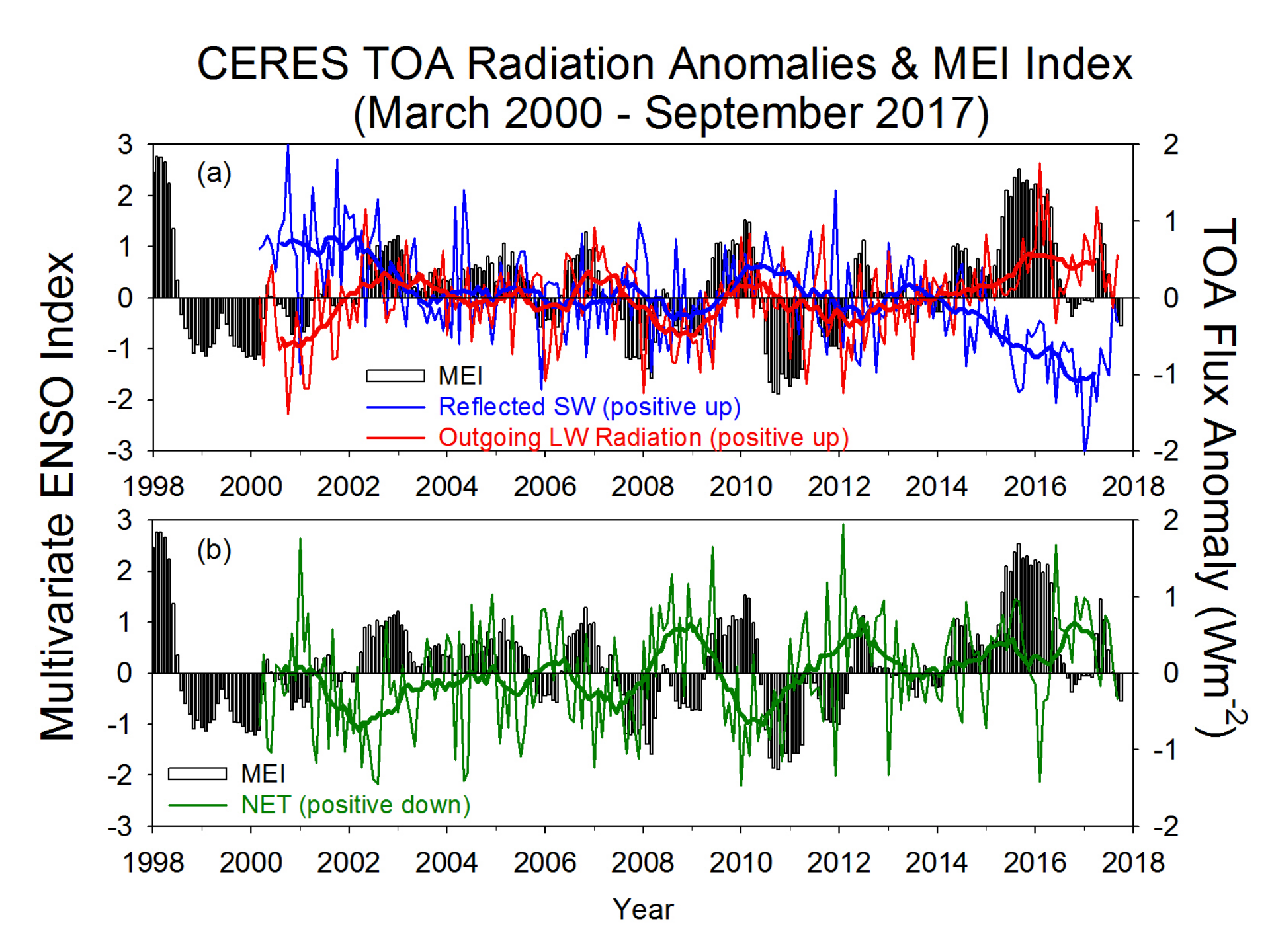
CERES TOA Radiation Anomalies & MEI Index
(March 2000 - September 2017)
(a)
MEI
Reflected SW (positive up)
Outgoing LW Radiation (positive up)
(b)
MEI
NET (positive down)
Multivariate ENSO Index
TOA Flux Anomaly (Wm-2)
Year
1998
2000
2002
2004
2006
2008
2010
2012
2014
2016
2018

Lagged Regressions in TOA Radiation Anomalies Against Nino3.4 Anomalies

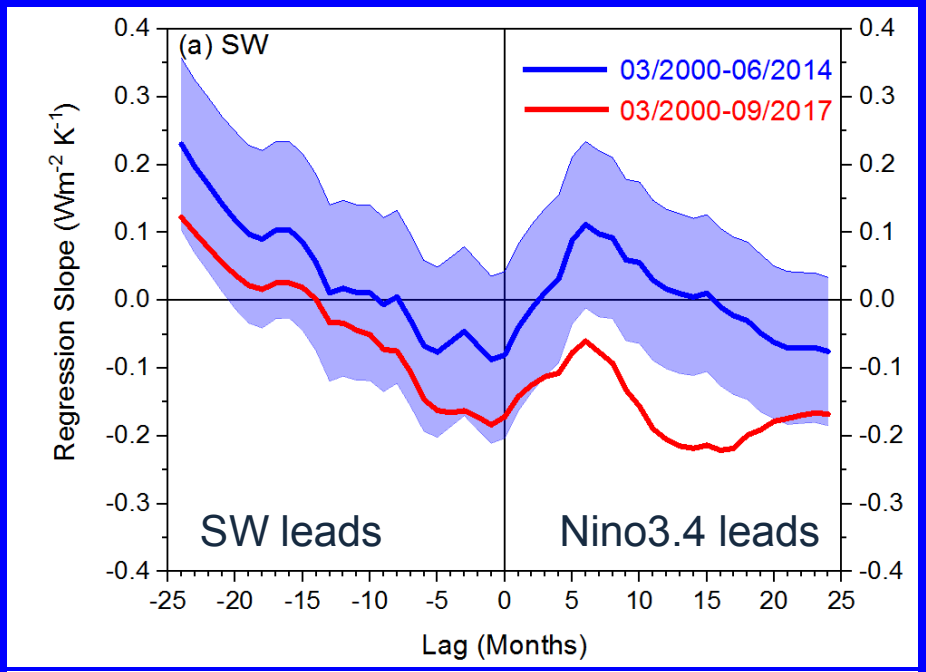

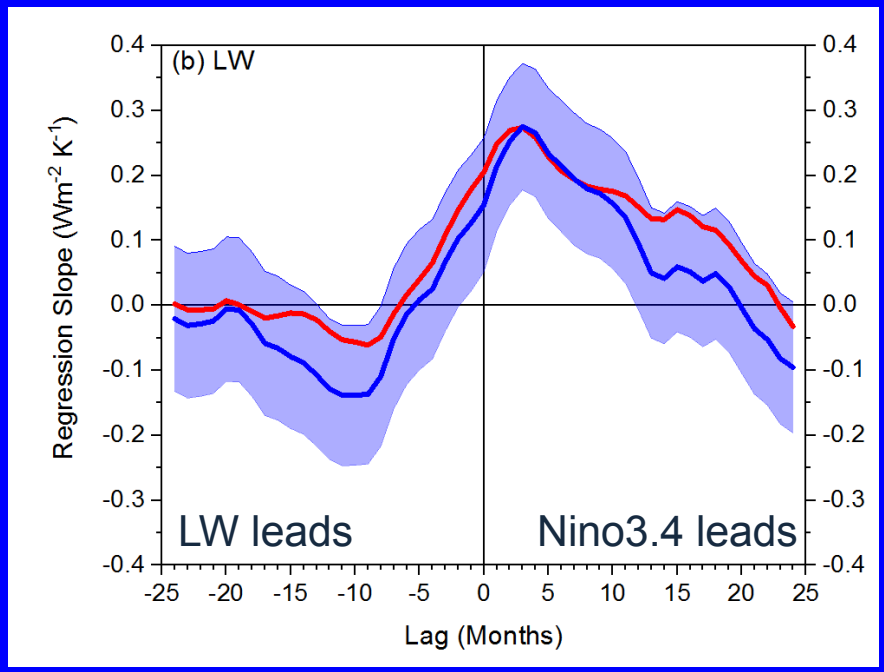

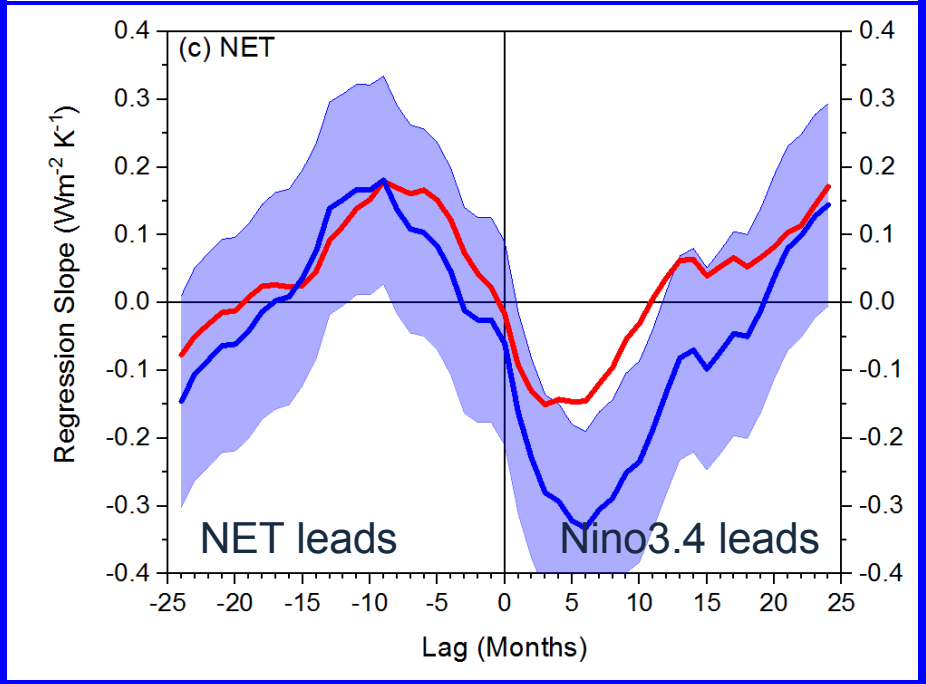

- An El Niño at zero lag is typically preceded by heat uptake into the system and followed by release of heat out of the system.
- This pattern is mainly driven by OLR.
- Unprecedented negative SW anomalies following the 2015-2016 El Niño significantly alter the TOA net radiation response to ENSO (red line).

⇒ Less heat release out of the system following El Niño.

Zonal Mean Differences in TOA Radiation (07/2014-06/2017) minus (07/2000-06/2014)

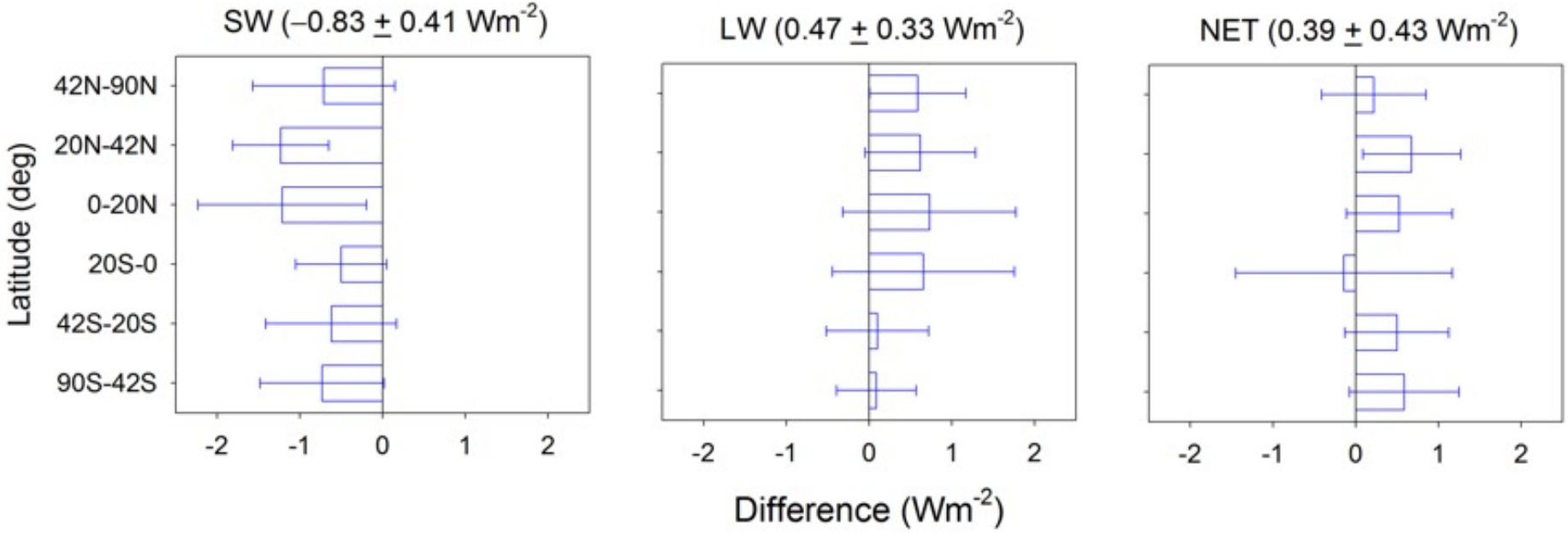

Regional Mean Differences in TOA Radiation (07/2014-06/2017) minus (07/2000-06/2014)

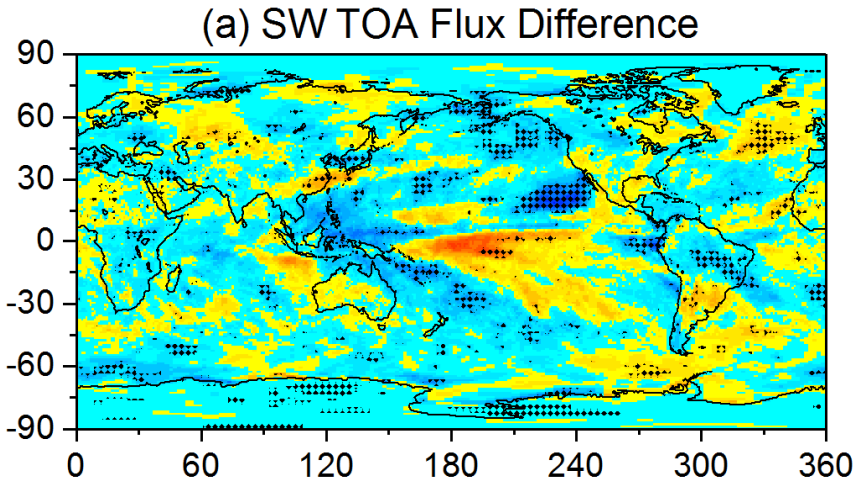

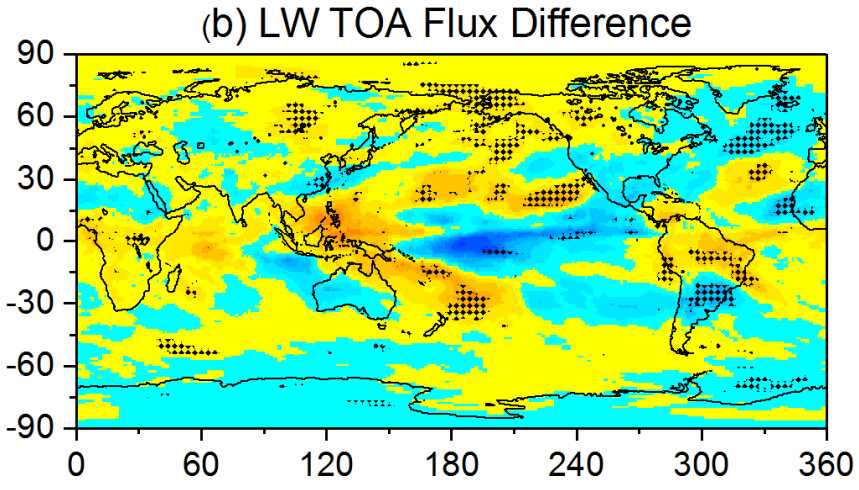

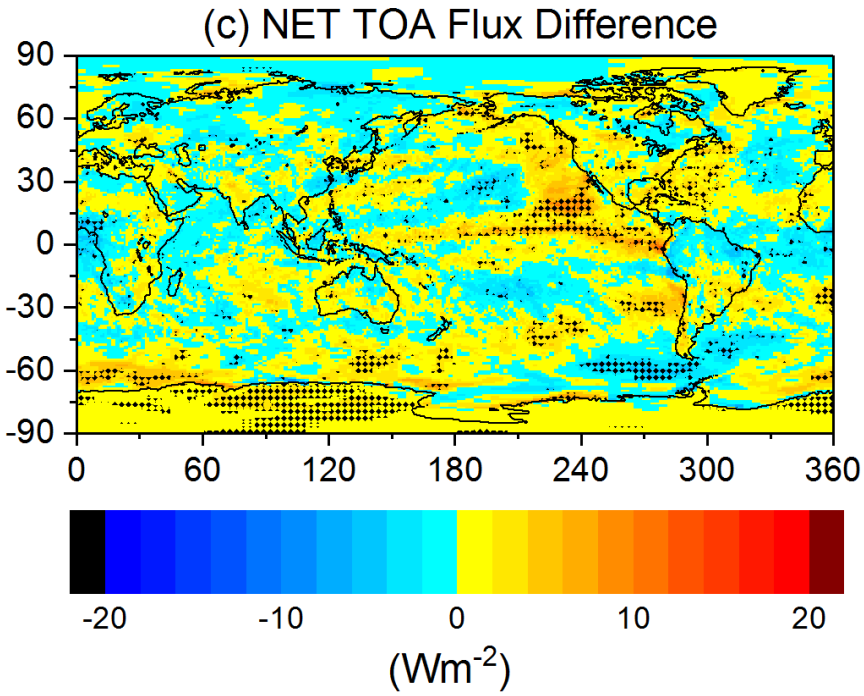

- TOA flux difference pattern in the tropics is dominated by ENSO.
- Substantial decrease in SW TOA flux over eastern and northern Pacific Ocean.

CERES-PRP (Partial Radiative Perturbation) Methodology

- Goal is to decompose the total radiative flux anomalies into the contributions from individual variables (e.g., cloud, surface, aerosol, etc., parameters).

$$\partial F^f_{\Delta x} = F(x, y_1, ..., y_N) - F(\overline{x}, y_1, ..., y_N) + O^f(\Delta x) \quad (1)$$

- Flux (F) difference of monthly means (x,y) and climatological monthly means ($\overline{x}$,$\overline{y}$)

Can also compute the same thing relative to a different base state:

$$\partial F^b_{\Delta x} = F(x, \overline{y_1}, ..., \overline{y_N}) - F(\overline{x}, \overline{y_1}, ..., \overline{y_N}) + O^b(\Delta x) \quad (2)$$

- $O^f(\Delta x)/O^b(\Delta x)$: truncation error

Reduce error by averaging the forwards (f) and backwards (b) difference

$$\partial F_{\Delta x} = \frac{\partial F^f_{\Delta x} + \partial F^b_{\Delta x}}{2} + O(\Delta x^2) \quad (3)$$

- From monthly-mean inputs, climatologies are constructed and the variables combined to make the 4 sets of inputs $\rightarrow$ Fu-Liou radiative model

PRP SW TOA Flux & SST Difference (07/2014-06/2017) minus (07/2000-06/2014)

PRP SW Flux Diff (Low cld frac contrib)

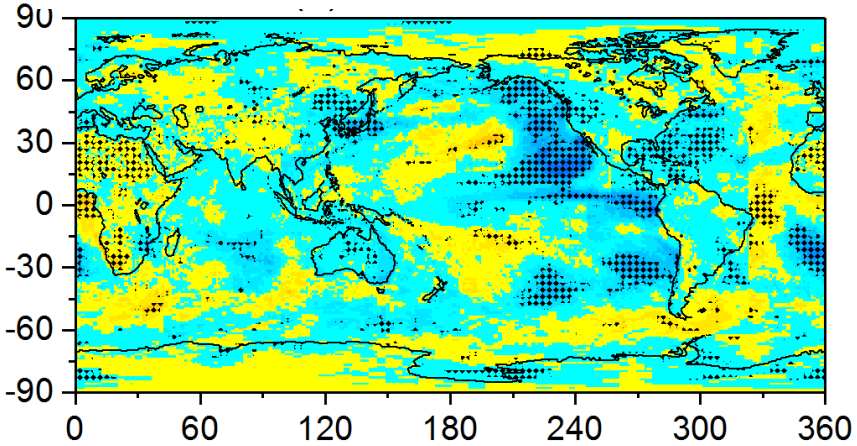

PRP SW Flux Diff (Mid+High cld frac contrib)

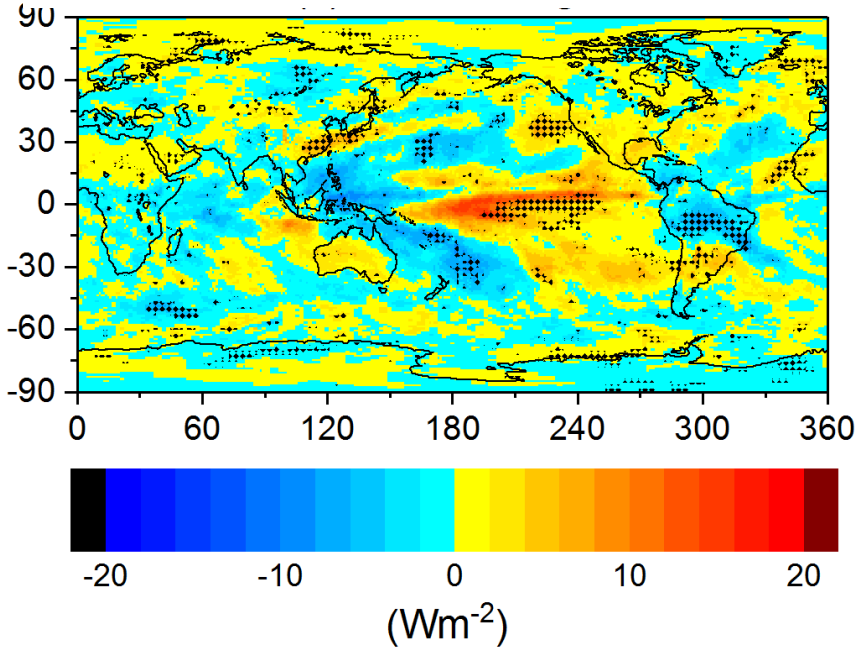

SST Difference

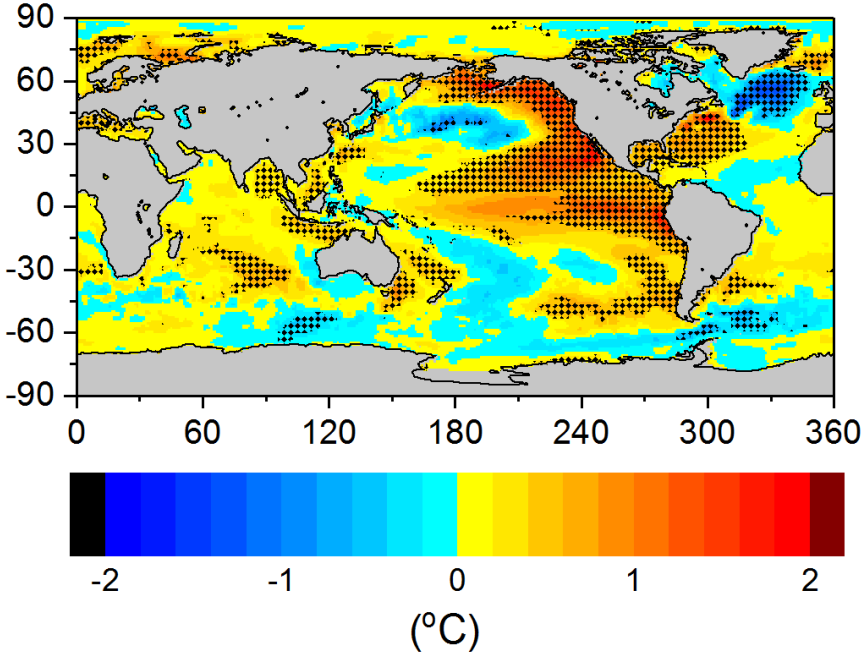

- Significant reduction in SW TOA flux due to reduction in low cloud along Eastern Pacific Ocean.

- Low cloud reduction occurs in regions of significant SST warming.

TOA SW & LW Comparisons Between CERES and GEOS-5 AMIP Simulations

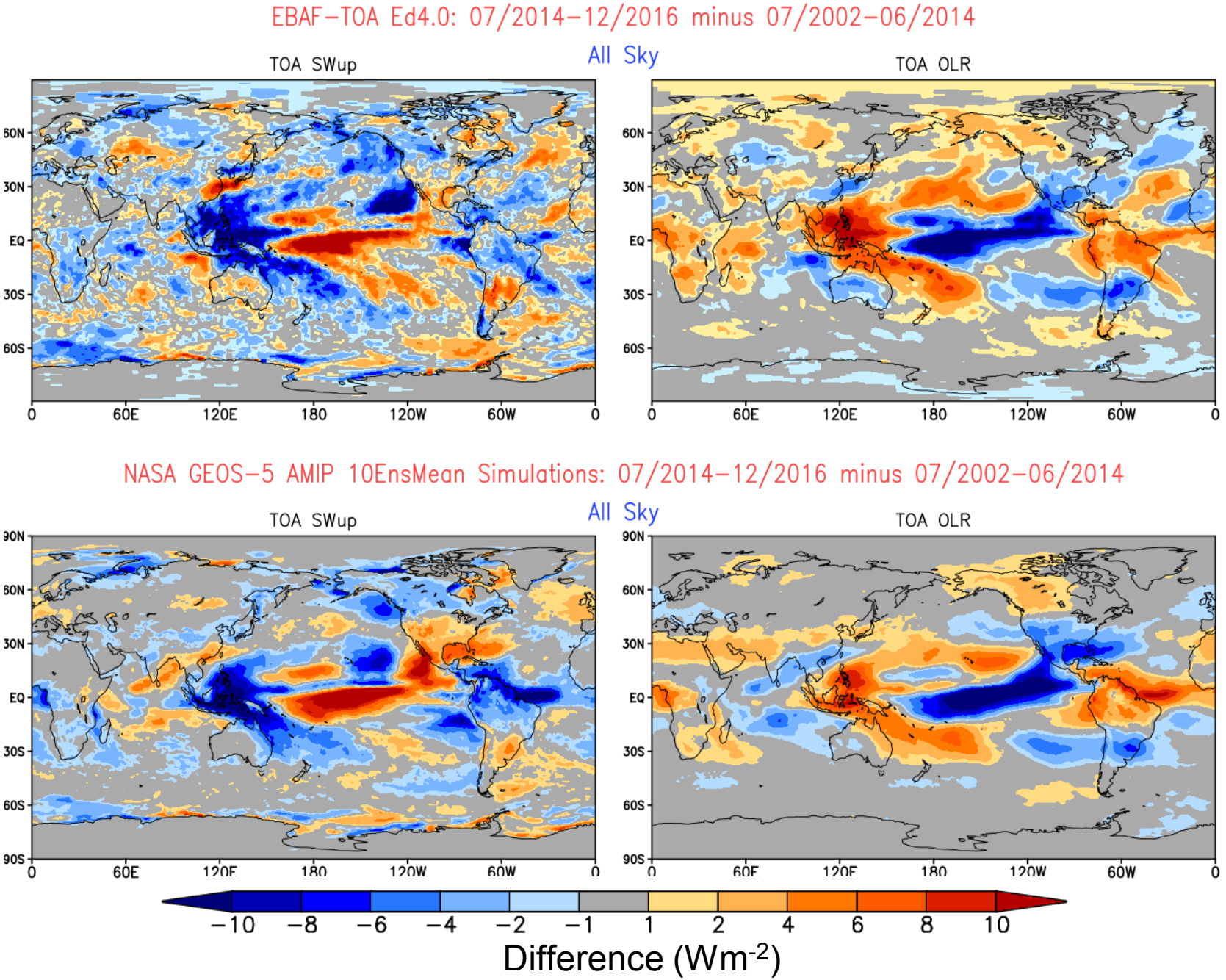

Low Cloud Fraction: 07/2014–12/2016 minus 07/2002–06/2014

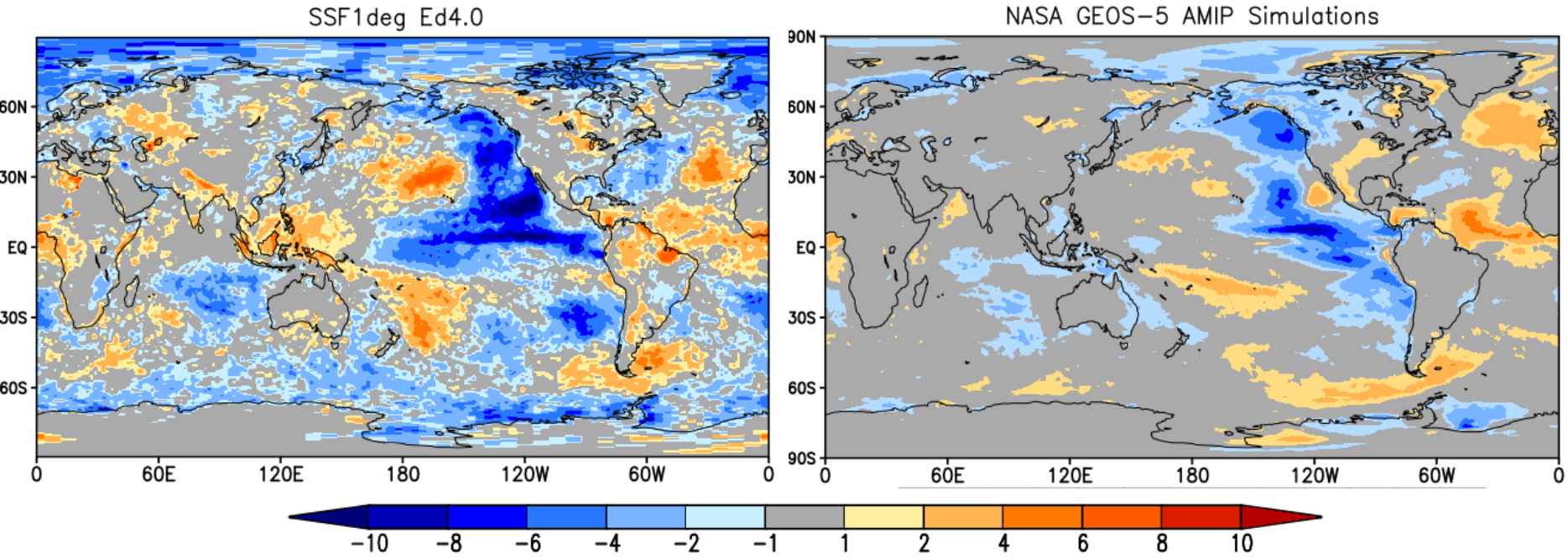

- Low cloud fraction in GEOS-5 AGCM is defined as cloud fraction from surface to 700hPa
- Reference of the GEOS-5 AMIP simulations:
  - Collow et al (2017), a GMAO technical report (https://gmao.gsfc.nasa.gov/pubs/docs/Collow963.pdf)

Clear-Sky SW TOA Flux & AOD Diffs: (07/2014-06/2017) minus (07/2000-06/2014)

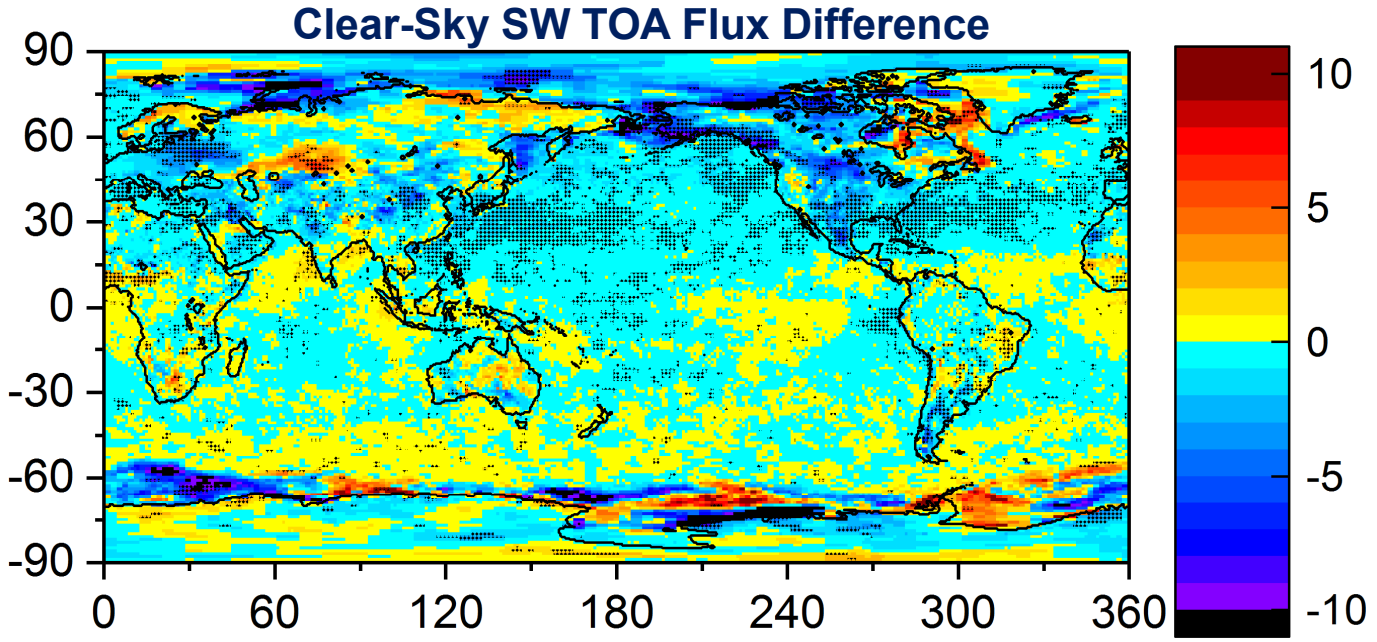

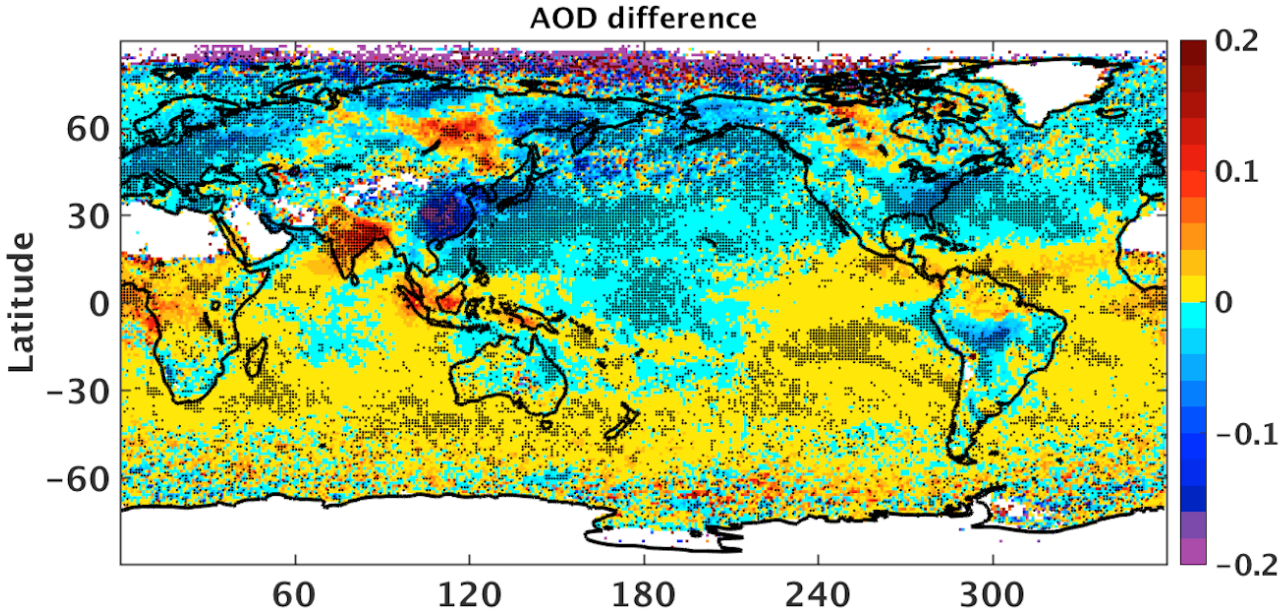

Conclusions

- Latter part of CERES record characterized by significant decrease in SW TOA flux due to a decrease in low cloud fraction over the Eastern Pacific.
- These changes coincide with shift in sign of PDO to positive, and anomalous SST pattern over E. Pacific.
- Largest uncertainty in projecting climate response to doubling CO_2 is associated with low cloud feedback.
- Observed low cloud fraction changes provide an unprecedented opportunity for testing climate models (e.g., AMIP simulations vs observations).

Thank You!

NPP Launch Arc, Oct. 28, 2011